44th AIAA/ASME/ASCE/AHS Structures, Structural Dynamics, and Materials Confere
7-10 April 2003, Norfolk, Virginia

AIAA 2003-1942

Flutter Characteristics of an Over-the-Wing Engine Mount Business-Jet Configuration

Michimasa Fujino* and Hiroki Oyama†
Honda R&D Americas, Inc.
6423B Bryan Blvd., Greensboro, NC 27409, USA
Hideo Omotani‡
Honda R&D Wako Research Center
1-4-1 Chuo, Wako-shi, Saitama, Japan

Abstract

Mounting engines on the wing causes complex wing flutter characteristics. The location of the engine mass and the stiffness of the pylon relative to the wing are important in preventing hazardous wing flutter. In addition, if the nacelles are installed over the wing, aerodynamic interference between the wing and the nacelle may cause unfavorable flutter characteristics, in particular, at transonic speeds. The flutter characteristics of an over-the-wing engine mount configuration obtained from theoretical analyses and low speed and transonic wind tunnel tests, are presented.

Nomenclature

c	wing local chord
b	wing semi-chord at 75% wing span
D	dissipation function
g	structural damping
g_i	structural damping for ith mode
k	reduced frequency
M	Mach number
M_i	generalized mass for ith mode
m(x,y)	mass of wing per unit area
n	number of modes
$\Delta p(x,y,t)$	lifting pressure at point (x,y) on wing at time t
$\Delta p_j(x,y,k,M)$	lifting surface pressure at point (x,y) on wing at k and M
Q_i	generalized force for ith degree of freedom
q_i	ith generalized coordinate
s	wing semi-span
T	kinetic energy
t	time
U	potential energy
V	free stream velocity
v	volume of a conical frustum having exposed wing root chord as base diameter, wing tip chord as upper diameter, and exposed wing semispan as height
w(x,y,t)	displacement of oscillating wing normal to x,y plane
$w_i(x,y)$	deflection shape of ith mode
$w_{0,i}$	amplitude for ith mode (complex)
x	streamwise coordinate
y	spanwise coordinate
δ_{ij}	Kronecker delta
μ	mass ratio, $m/\rho v$
ρ	density
ω	circular frequency
ω_h	uncouple circular frequency of wing 1st bending
ω_p	uncouple circular frequency of pylon pitching
ω_{SB}	uncouple circular frequency of pylon side-bending
ω_Y	uncouple circular frequency of pylon yaw
ω_i	circular frequency of ith mode
ω_α	uncouple circular frequency of wing 1st torsion

* Chief Engineer
†‡ Principal Engineer

Introduction

Small business jets are becoming very popular among business people. Market surveys show that demand for comfort, in particular, a large cabin, is critical to the success of business-jet development. Mounting the engines on the wing instead of the fuselage is one way to maximize cabin size by removing the engine support structure from the fuselage.

Recent research by Honda R&D shows that an optimum over-the-wing engine mount configuration minimizes aerodynamic interference at transonic speeds and reduces wave drag such that the range parameter for the over-the-wing engine mount configuration is about five percent higher than that of the conventional

Copyright © 2003 by the American Institute of Aeronautics and Astronautics, Inc. All rights reserved.

rear-fuselage engine mount configuration (ref. 1).

Mounting the engine on the wing, however, significantly changes the vibration characteristics of the original wing and, as a result, influences the aeroelastic characteristics (e.g. ref 2, 3). In addition, the nacelle aerodynamic load and interference may affect the flutter characteristics (e.g., ref.4). Positioning the engine ahead of the elastic axis of the wing to increase the flutter speed is a well-known design rule, which has a marked effect on the configuration of modern transport aircraft. For the present over-the-wing engine mount configuration, however, the engine is positioned aft of the elastic axis of the wing and the aeroelastic characteristics are, therefore, considered to be critical. Also the aerodynamic effect on the flutter characteristics induced by having the engine nacelle positioned over the wing must be carefully evaluated, especially in the transonic flight regime. It is necessary to validate these characteristics for the present over-the-wing engine nacelle configuration.

In the present study, the engine location relative to the wing was first systematically varied and the effect on the flutter speed was studied theoretically and in the low speed wind tunnel tests. (The engine pylon is rigid in this study.) The general tendencies were evaluated using a cantilever-wing flutter model. The study determined the effect of the chordwise and spanwise location of the engine on the flutter speed.

The pylon stiffness was then varied to alter the side-bending frequency, yawing frequency, and pitching frequency of the engine-pylon mode. The effects on the flutter characteristics of the over-the-wing engine mount configuration were thus quantitatively evaluated. The results show that the flutter characteristics change at a certain frequency ratio.

To investigate the flutter characteristics under the aerodynamic influence of the nacelle for the over-the-wing engine mount configuration, transonic flutter tests were also conducted. These tests show that there is no large flutter speed reduction at the transonic dip or undesirable flutter characteristics for the over-the-wing engine mount configuration.

Analysis

ERIN-Code

To study the flutter characteristics of the over-the-wing engine mount configuration, the ERIN Code was used. The ERIN Code, an integrated flutter design and analysis program developed by the first and the second author was used (Fig.1). The code consists of three

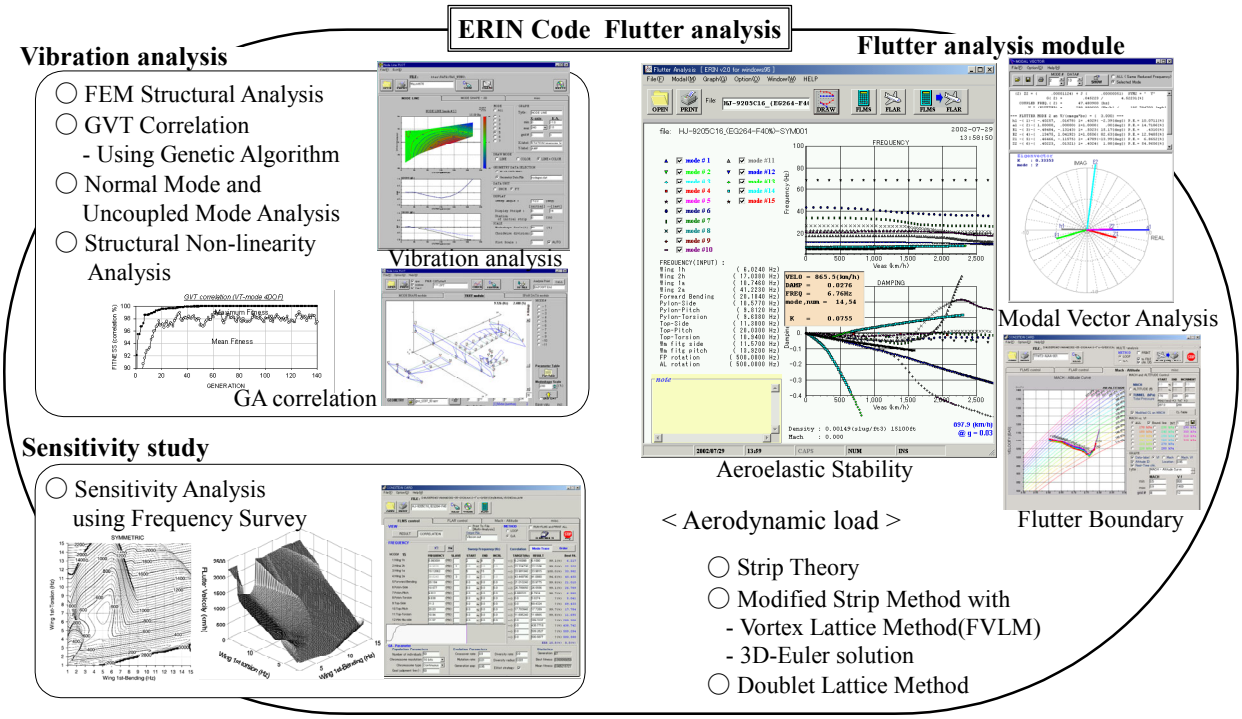

Fig.1 ERIN Code

major modules: flutter analysis, vibration analysis, and sensitivity analysis. The flutter analysis module is used to compute the U-g and U-f plots and the flutter speed

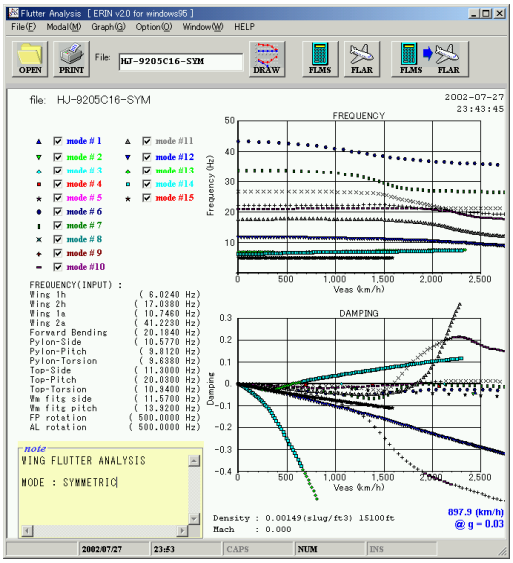

Fig.2 Flutter analysis module

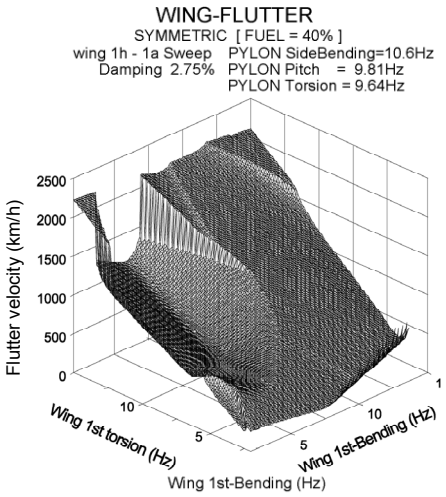

Fig.3 Sensitivity analysis module

(Fig.2). The vibration analysis module is used to establish the structural model employed in the flutter analysis. The sensitivity analysis module is used to evaluate the influence of each frequency on the flutter modes such that the flutter characteristics can be better understood. The frequency of each mode can be automatically swept and the corresponding flutter speeds are displayed, as shown in Fig.3.

The ERIN Code is a Microsoft Windows™ -based program that has an extensive interactive user interface. For example, by pointing with the mouse at a curve in a U-g plot, the reduced velocity, damping, mode vectors, etc. are displayed in a pop-up window (Fig.4). Mode vectors, which are displayed in a pop-up windows, are very useful for studying flutter modes.

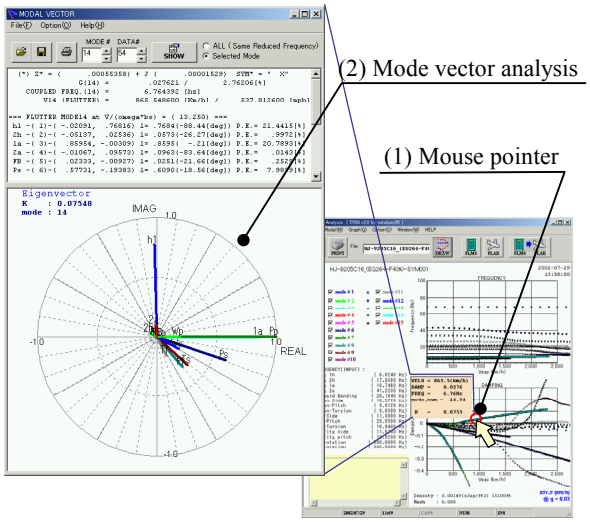

Fig.4 Interactive user interface of ERIN Code

Flutter Equations

The flutter equations are obtained from Lagrange's equations of motion. Lagrange's equations may be written in the form

$$\frac{d}{dt}\left(\frac{\partial T}{\partial \dot{q}_i}\right)+\frac{\partial U}{\partial q_i}+\frac{\partial D}{\partial \dot{q}_i}=Q_i \quad (i=1,2,\cdots,n) \qquad \text{----- (1)}$$

Assuming that the oscillatory deflection $w(x,y,t)$ of the wing can be represented by a linear combination of n mode shapes $w_i(x,y)$

$$w(x,y,t)=\sum_{i=1}^{n} w_i(x,y)w_{0i}e^{i\omega t}=\sum_{i=1}^{n} w_i(x,y)q_i(t) \qquad \text{--- (2)}$$

The kinetic energy of the oscillating wing is

$$T=\frac{1}{2}\sum_{i=1}^{n}\sum_{j=1}^{n}\dot{q}_i\dot{q}_j\iint_s m(x,y)w_i w_j\,dxdy \qquad \text{-- (3)}$$

If $w_i(x,y)$ are the normal modes of the wing in a vacuum,

$$\iint_s m(x,y) w_i w_j dxdy = M_i \delta_{ij} \quad \text{----------(4)}$$

and

$$T = \frac{1}{2}\sum_{i=1}^{n} M_i \dot{q}_i^2 \quad \text{----------(5)}$$

The potential energy U can be represented as

$$U = \frac{1}{2}\sum_{i=1}^{n} \omega_i^2 M_i q_i^2 \quad \text{----------(6)}$$

The dissipation function for the structural damping is

$$D = \frac{1}{2}\sum_{i=1}^{n} M_i g_i \frac{\omega_i^2}{\omega} \dot{q}_i^2 \quad \text{----------(7)}$$

Substituting equations (5), (6), and (7) into equation (1) and assuming harmonic motion leads to

$$\left[\frac{\omega_i^2}{\omega^2}(1+ig_i)-1\right]\omega^2 M_i q_i = Q_i \quad \text{----------(8)}$$

The generalized forces are

$$Q_i(t) = \iint_s \Delta p(x,y,t) w_i(x,y) dxdy \quad \text{----------(9)}$$

Assuming motion of very small amplitude permits Δp to be expressed as the sum of the contributions from each mode:

$$\Delta p(x,y,t) = \sum_{j=1}^{n} \Delta p_j(x,y,k,M) e^{i\omega t} \quad \text{----------(10)}$$

where $\Delta p_j(x,y,k,M)$ is the lifting surface pressure at point (x,y) on the wing caused by the motion of the wing in the jth mode.

The equation of motion (8) is therefore homogeneous in the n q_j's, which leads to an algebraic eigenvalue problem. The requirement for nonzero solutions is that the determinant of the coefficients, which is called the flutter determinant, must vanish. The flutter determinant is solved by the k-method.

Aerodynamic Load

There are three methods of aerodynamic loads calculation in the ERIN Code; strip method (ref.5), modified strip method (ref.6), and doublet lattice method (ref.7). In this study, the modified strip method (MSM) and the doublet lattice method (DLM) were used. When the modified strip method is used, the lift-curve slope and aerodynamic center are corrected using the steady-state Euler solution coupled with a boundary-layer method (refs. 8, 9, and 10) for transonic flutter analyses and using a vortex lattice method (FVLM Code, which was developed by Honda R&D) for low-speed flutter analyses. The downwash collocation point, where the downwash induced by the aerodynamic load is set to be equal to the kinematic downwash, is modified accordingly.

Flutter Analysis

A vibration analysis based on a finite element method was performed using the measured stiffness and weight properties. Ground vibration tests of the flutter models were also conducted to refine the structural model. The generalized mass and each frequency obtained from the vibration analysis were input into the flutter analysis module of the ERIN Code. To perform the flutter analysis, the wing 1st bending, wing 2nd bending, wing 1st torsion, wing 2nd torsion, engine-pylon pitch, engine-pylon yaw, and engine-pylon side bending are considered for the cantilever condition. For the free-free mode condition, the fuselage rigid-roll mode and heaving mode are also considered.

Experiment

Low Speed Wind Tunnel Test

To evaluate the basic flutter characteristics of the over-the-wing engine mount configuration, a tunnel test was conducted in the Honda Low Speed Wind Tunnel (HLWT), which has a 5 m x 3.5 m test section and a closed return (Fig.5). The 1/4-scale model employed

Fig.5 Honda low speed wind tunnel

spar-strip construction. The aluminum spar plus flange section provided the required stiffness distribution in bending and torsion. The strips were made of rapid prototyping resin and lead and tungsten weights were installed in each strip to yield the required mass, center of gravity, and moment of inertia properties. The gaps between the strips were aerodynamically sealed with sponge rubber (Fig.6).

Two types of model supports, mounted on the ceiling, were used: a cantilever support and a hinge type-support (Fig.7) to obtain free rolling motion of the fuselage such that antisymmetric flutter could occur. The impact hammering method as well as natural wind-tunnel turbulence were used as the excitation force to initiate flutter, as required.

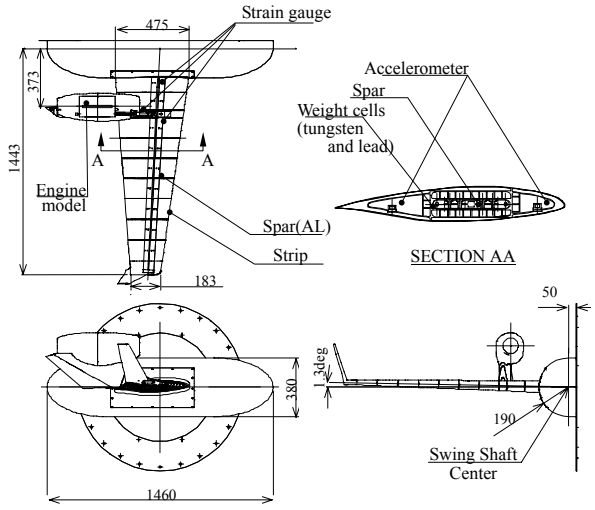

Fig.6 1/4-scale low speed wing flutter test model

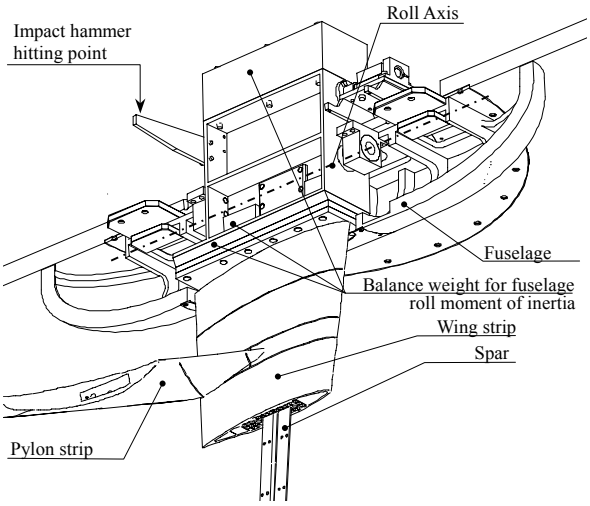

Fig. 7 Model support mechanism for free-free antisymmetric wing flutter test

Transonic Wind Tunnel Test

Transonic tests were conducted in the National Aeronautical Lab (NAL). Two types of transonic wind tunnel were used for the tests. One is the transonic flutter wind tunnel, which is a blow-down wind tunnel having a 0.6 m x 0.6 m test section (Fig.8). The tunnel is capable of operating at total pressures from 147 to 392 kPa and at Mach Numbers from 0.5 to 1.2. The tunnel is equipped with a quick model retraction system that withdraws the model from the test section when flutter occurs (Fig.9).

The other is the transonic wind tunnel, which is a closed return wind tunnel having a 2 m x 2 m test section (Fig.10) and the tunnel is capable of operating at total pressure from 50 kPa to 150 kPa and at Mach

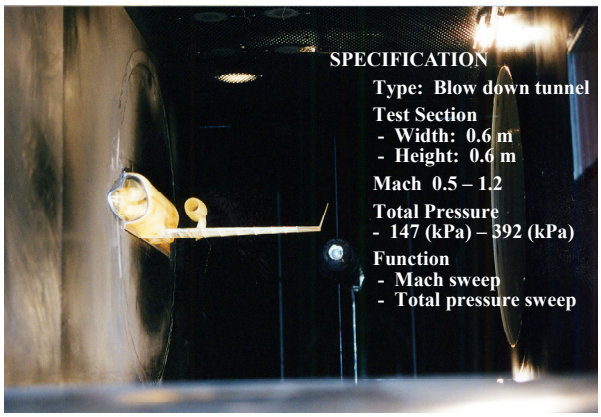

Fig.8 NAL transonic flutter wind tunnel

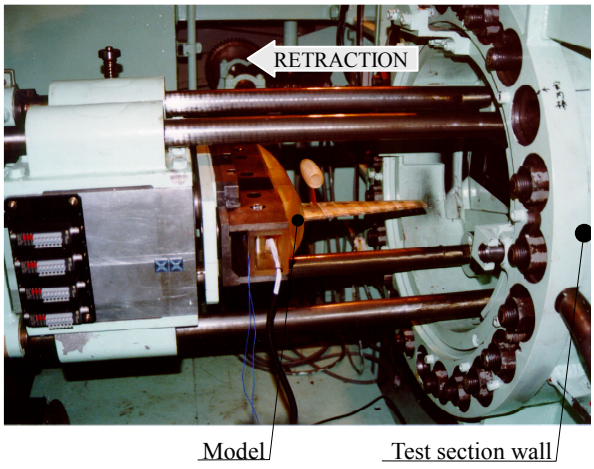

Fig.9 Model retraction system

number from 0.5 to 1.4.

A 1/20-scale model (Fig.11, 12) was used for tests in the 0.6 m x 0.6 m transonic flutter wind tunnel and a 1/6-scale model (Fig.13) was used for tests in the 2 m x 2 m transonic wind tunnel. The models were of spar-strip construction. Each strip was made of rapid prototyping resin and the steel spar provided the required stiffness properties in bending and torsion scaled from the actual wing. The required mass and inertial properties were provided by tungsten weights in each strip. Flow-through nacelles were used.

The models were cantilever supported from the sidewall (transonic flutter wind tunnel) or from the ceiling (2 m x 2 m transonic wind tunnel). In both tests, natural wind-tunnel turbulence was used as the excitation force to initiate flutter.

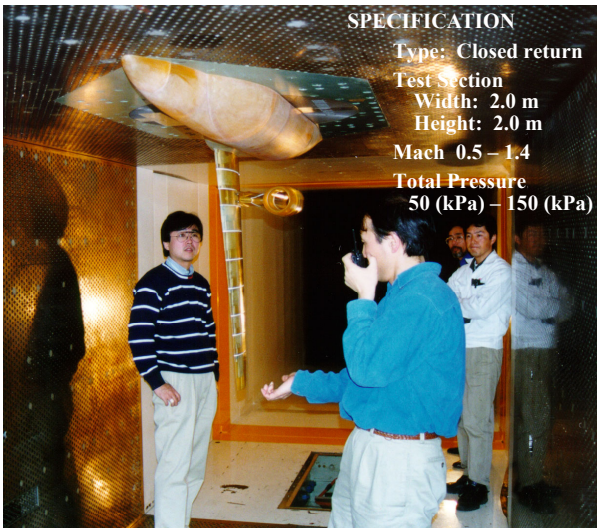

Fig.10 NAL 2m x 2m transonic wind tunnel

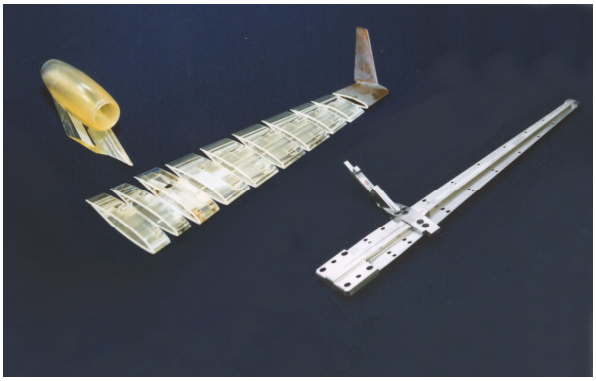

Fig.11 1/20-scale transonic wing flutter test model

Instrumentation

In both tests, strain gauges were mounted near the root of the wing and on the pylon spar to indicate deflection in bending and torsion for each mode. Strain gauges were also mounted on the pylon spar to indicate pylon bending and pylon pitching. The strain gauge signals were continuously recorded by the data acquisition system and were Fast Fourier Transformed to obtain the power spectrum density. Response time history was also plotted by a pen-recorder allowing the model response to be monitored in real time (Fig.14).

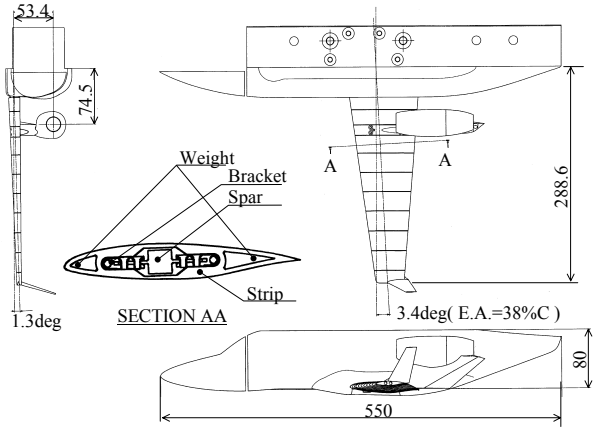

Fig.12 1/20-scale transonic wing flutter test model (Three view drawing)

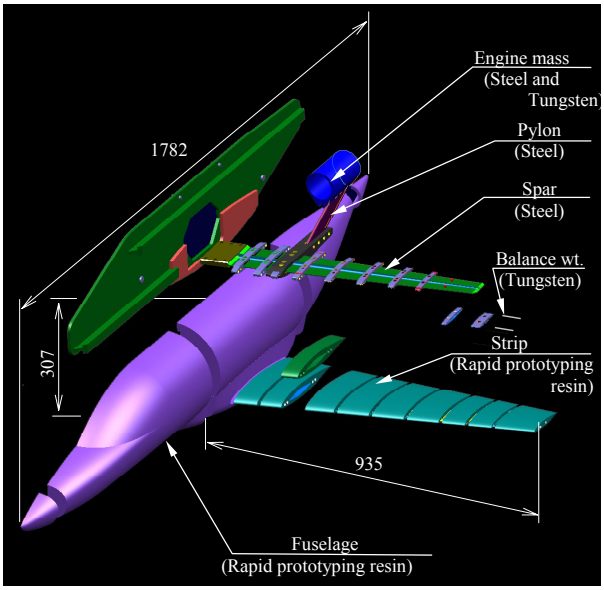

Fig.13 1/6-scale transonic wing flutter test model

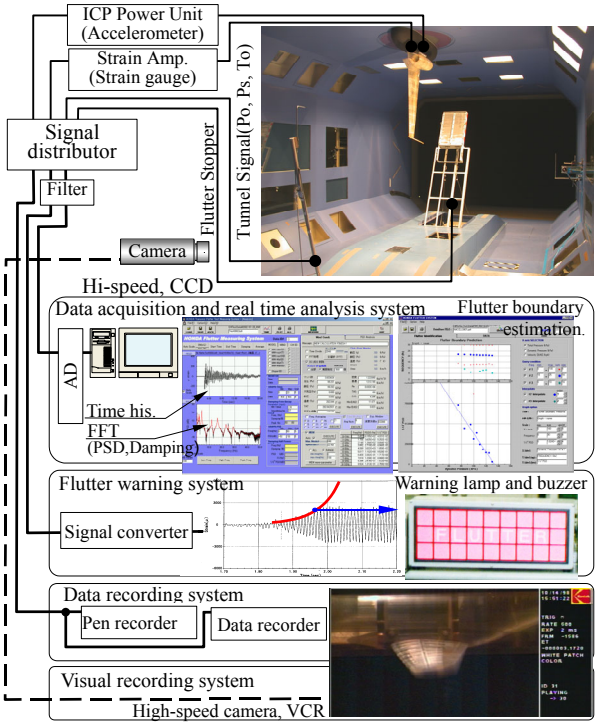

Fig.14 Flutter test instrumentation

Two subcritical response methods were used to predict model flutter characteristics; the Power Spectrum Density (PSD) method and the Peak-Hold method. The PSD method was implemented as shown in Fig.15. The power spectrum density obtained from the model dynamic response has a peak for each structural mode, which yields the structural damping. As illustrated in Fig.15, the structural damping is equal to the frequency bandwidth, taken at the half-power point, divided by the

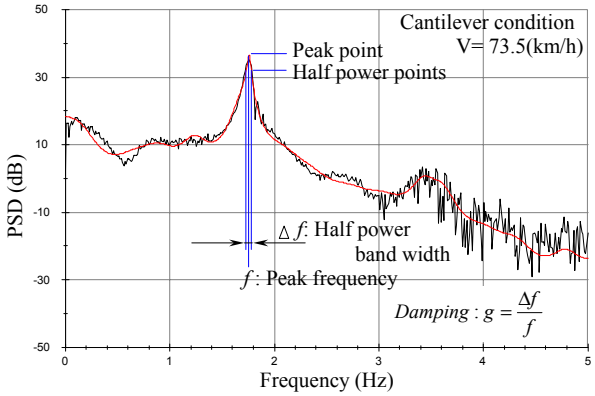

Fig. 15 PSD method

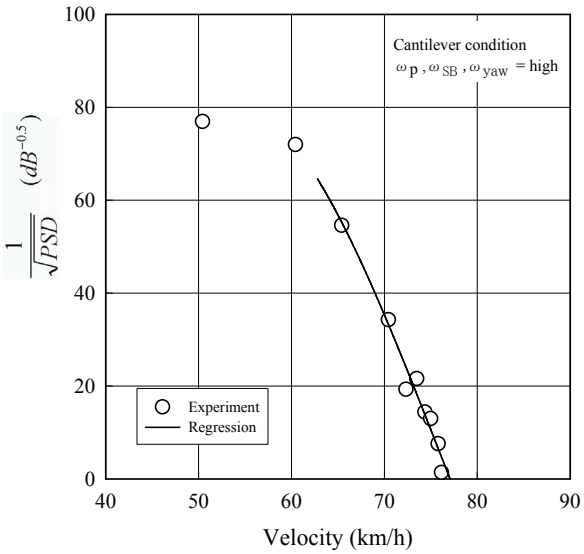

Fig.16 Peak-Hold method

mode frequency. The Peak-Hold method was implemented as shown in Fig.16. The reciprocal of the peak spectrum amplitude is proportional to the damping ratio and is used to evaluate flutter stability. For the PSD method, the flutter points were determined by extrapolating the structural damping. For the Peak-Hold method, the flutter points were determined by extrapolating the reciprocal of the peak spectrum amplitude.

Visual records of the model behavior were also provided by a digital high-speed camera capable of 1000 frames per second (Fig.17).

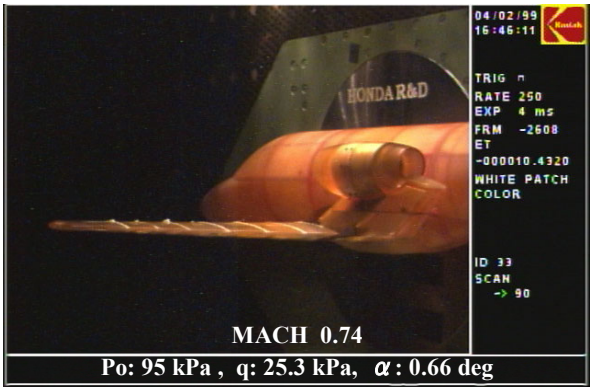

Cantilever condition
1/6-scale transonic wind flutter test

Fig.17 Visual records by digital high-speed camera

Results and Discussion

Effect of Engine Location

To investigate the effect of the engine location on the flutter speed, a test using a cantilever model was conducted in the Honda Low Speed Wind Tunnel (Fig.18).

Fig.18 Low speed wing flutter test

The effects of chordwise and spanwise engine location on flutter speed are shown in Fig.19. The elastic axis of the wing coincided with 32-percent chord. The flutter speed is higher when the engine is located ahead of the elastic axis and this tendency becomes stronger as the engine moves outboard. Conversely, the flutter speed is lower when the engine is installed aft of the elastic axis.

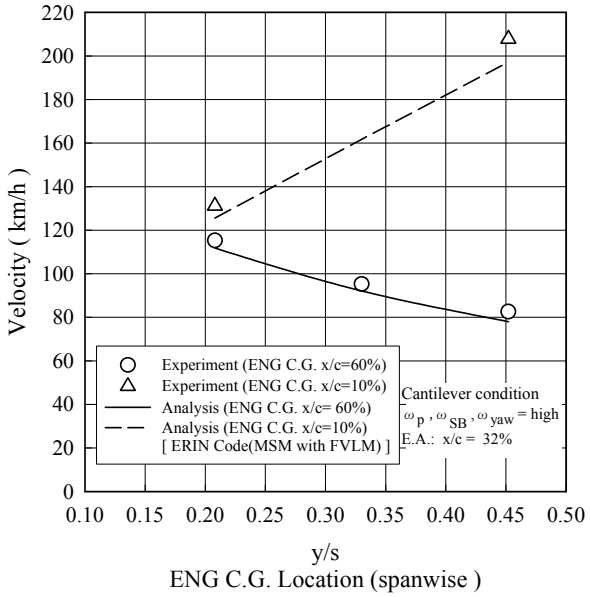

Fig.19 Effect of engine location on flutter speed

The flutter characteristics are less sensitive for the inboard engine installation.

Comparisons of the ERIN Code predictions and the experimental results shows good agreement (Fig.19).

Effect of Engine Pylon Side-Bending, Yawing and Pitching

The engine-pylon side-bending, yawing and pitching modes are important for the wing flutter characteristics. These modes were studied using the ERIN Code and in the wind tunnel.

Flutter analyses were performed to evaluate the engine-pylon side-bending effect on the flutter speed (Fig.20). In this example, the engine was located at 33-percent span and 60-percent chord. The flutter speed is highest when the side-bending frequency is close to the wing uncouple 1st torsion frequency. A result from the low speed wind tunnel test in the HLWT is included in Fig.20. The ERIN Code predictions agree well with the measurements.

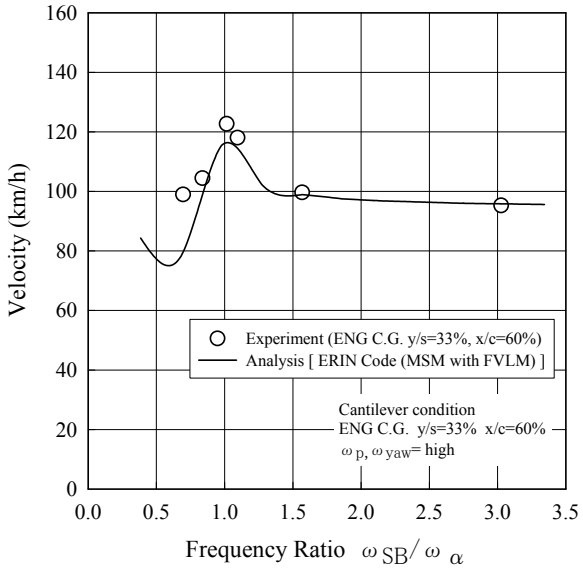

Fig.20 Effect of engine-pylon side-bending frequency

The results from theoretical flutter analyses and the test in the NAL 2 m x 2 m transonic wind tunnel using a 1/6-scale model (see Fig.10) are shown in Fig.21. In this case, the engine was located at 26-percent span and 135-percent chord, which corresponds to the optimum

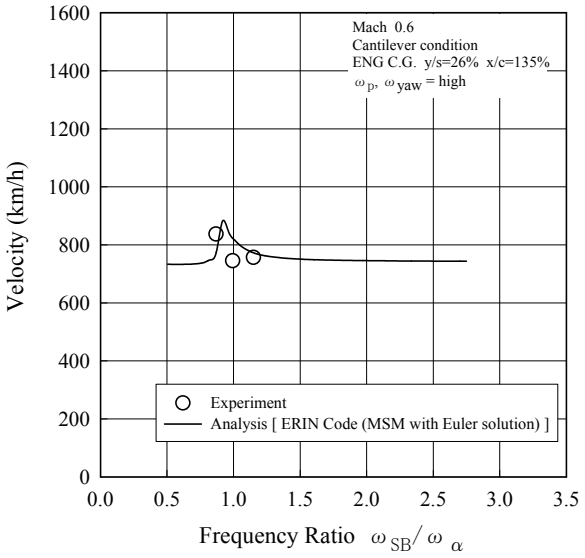

Fig.21 Effect of engine-pylon side-bending frequency
(1/6-scale model,EG location 26%span 135%chord)

(with respect to drag) over-the-wing engine mount configuration. Again the flutter speed is highest when the side-bending frequency is about 0.9 times the wing uncouple 1st torsion frequency. The ERIN Code predictions agree well with the measurements. The engine-pylon side-bending effects are similar for other spanwise engine locations.

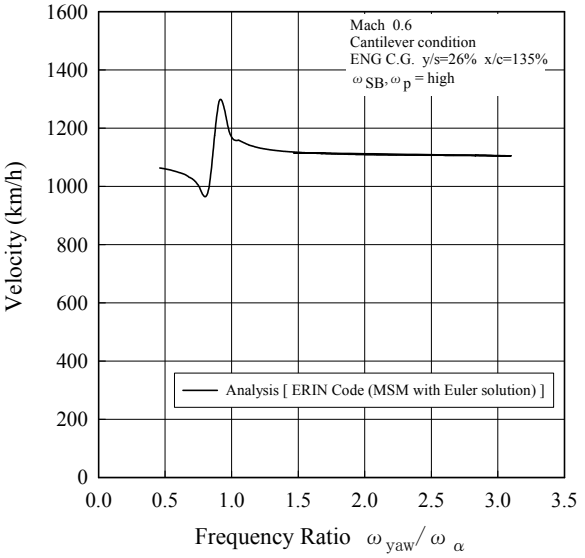

Fig.22 Effect of engine-pylon yawing frequency

The effect of engine-pylon yawing mode on flutter characteristics predicted using the ERIN Code is shown in Fig.22. The engine was located at 26-percent span and 135-percent chord. The flutter speed is highest when the engine-pylon yawing frequency is about 0.9 times the wing uncouple 1st torsion frequency and the flutter speed decreases below this frequency. This result is similar to that of the engine-pylon side-bending mode.

The effect of the engine-pylon pitching frequency on flutter speed is shown in Fig.23. The engine was located at 26-percent span and 135-percent chord. The ERIN Code analysis shows that the flutter speed is lowest when the engine-pylon pitching frequency is about 1.25 times the wing uncouple 1st bending frequency; the flutter speed increases above or below this frequency ratio. A corresponding test was also conducted in the NAL transonic flutter wind tunnel using a 1/20-scale model (see Fig.8) at a Mach number of 0.6. The agreement between the analysis and the tests is good. This tendency is similar for other spanwise engine locations.

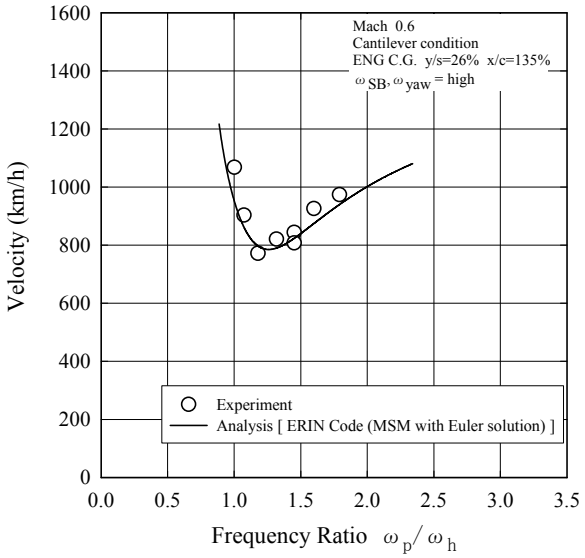

Fig.23 Effect of engine-pylon pitching frequency

Effect of the Aerodynamic Interference due to Nacelle Installation Over the Wing

Positioning the nacelle over the wing influences the

flow characteristics, in particular, in transonic speeds. The wave drag is reduced by locating the engine nacelle at the optimum location relative to the wing, as shown in ref 1. It is, however, possible that change in steady and unsteady aerodynamic loads due to the nacelle installation over the wing may alter the flutter characteristics at transonic speeds. Thus it is necessary to conduct a transonic flutter test to evaluate this configuration quantitatively.

The first transonic flutter test was conducted using a 1/20-scale model of the clean wing at the NAL transonic flutter wind tunnel (see Fig.8). The wing airfoil is a natural-laminar-flow airfoil developed by Honda R&D (ref.11). The results are shown in Fig.24. The lower limit of the transonic flutter boundary occurs at about M=0.71; the reduction of the flutter-speed index from the low speed value at M=0.6 is about 6 percent. The predicted flutter-speed index is also shown. The results from the ERIN Code using the modified strip method with the steady-state Euler solution agree well up to a Mach number of 0.75, above which the predicted flutter-speed index is higher than the experimental value because the Euler solution, which is used to correct the aerodynamic load on each strip, does not take into account boundary-layer separation. The results from the ERIN Code using the doublet lattice method also agree well with the experimental results except the transonic dip is not predicted because the doublet lattice method is a linear theory.

The second transonic flutter test was conducted using the wing with the over-the-wing engine nacelle. The engine was located at 26-percent span and 135-percent chord. The results are shown in Fig.25. The lower limit of the transonic flutter boundary occurs at about M=0.74; the reduction of the flutter-speed index from the low speed value at M=0.6 is about 10 percent, which is slightly larger than that for the clean wing configuration. The Mach number at which the lower limit of the transonic flutter boundary occurs for the over-the-wing engine mount configuration is 0.03 higher than that of the clean wing configuration. This occurs because the drag-divergence Mach number of the over-the-wing engine mount configuration is about 0.03 higher than that for the clean-wing configuration due to positive aerodynamic interference and it influences the flutter characteristic. The predicted flutter-speed index agrees well with the measurements except the ERIN Code predicts slightly higher Mach number at which the lower limit of the transonic flutter boundary occurs. The theoretical and experimental results show that the effect of the nacelle aerodynamic load on the flutter characteristics is small at transonic speeds. The aerodynamic load of the engine nacelle installed over-the-wing has little effect because the deflection of the inboard wing, where the engine is positioned, is small. In addition, the aerodynamic interference between the nacelle and the wing does not affect the flutter characteristics significantly.

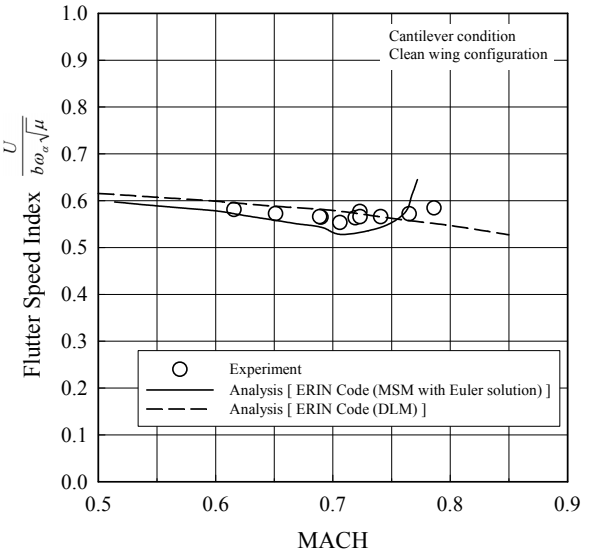

Fig.24 Transonic flutter characteristic of the clean wing configuration

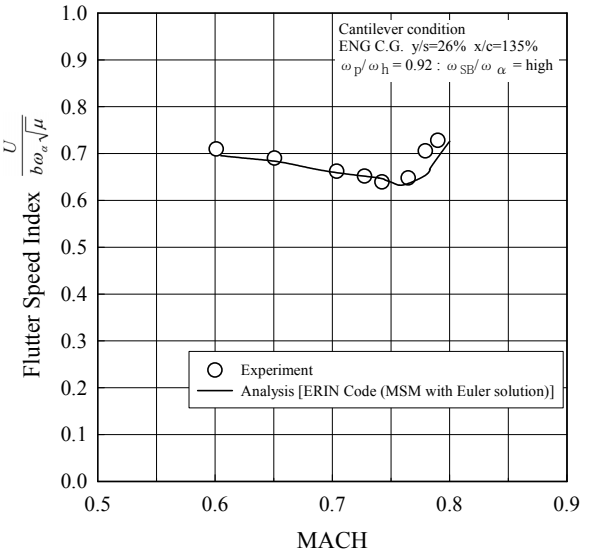

Fig.25 Transonic flutter characteristic of the over-the-wing engine mount configuration

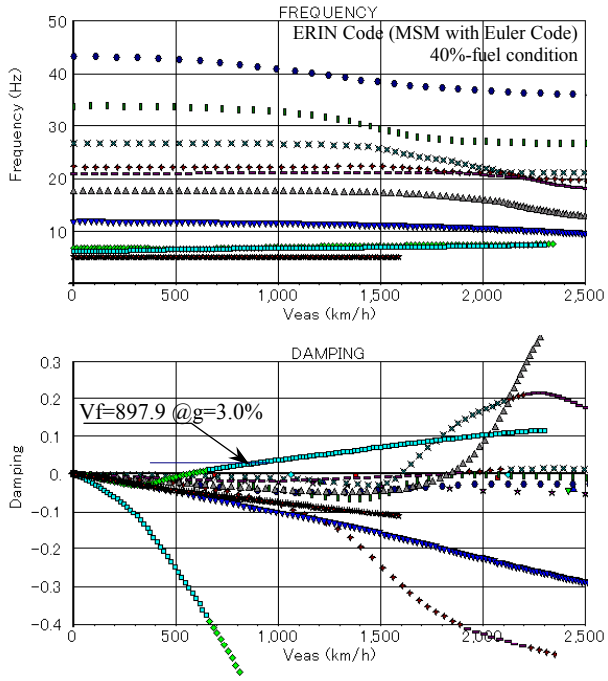

Fig.26 Flutter characteristic for free-free symmetric condition

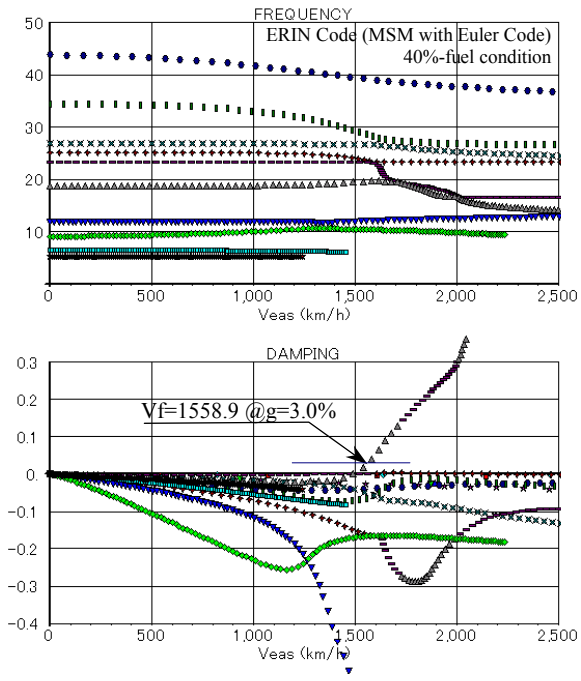

Fig.27 Flutter characteristic for free-free antisymmetric condition

Flutter Characteristics of Free-Free Mode

The flutter characteristics of the over-the-wing engine mount configuration must also be carefully evaluated under the free-free condition because the engines are located inboard of the node line for the wing 1st bending mode. The engines, located aft of the elastic axis of the wing, act as unbalance for the symmetric flutter condition and, therefore, the flutter speed tends to be lower. On the other hand, the engines act as mass balance for the antisymmetric condition and, thus, the flutter speed tends to be higher. These characteristics were quantitatively evaluated by analysis and experiment. An example of the U-g plots obtained from the ERIN Code analyses for the full-scale airplane are shown for the symmetric condition in Fig.26 and for the antisymmetric condition in Fig.27. The flutter speed for the antisymmetric mode is about 1.7 times higher than that for the symmetric mode. This result is quite different from that for the clean wing configuration. For the over-the-wing engine mount configuration, the symmetric condition is critical and must be evaluated carefully.

Accordingly, an antisymmetric flutter test using a 1/4-scale model with a hinge-type support (see Fig.7) was conducted in the Honda Low Speed Wind Tunnel. It should be noted that the model was supported from the tunnel ceiling and the rigid roll mode frequency is about 0.45 Hz, which was considered in the analysis. The results are shown in Fig.28. The antisymmetric flutter mode predicted by the ERIN Code agrees well with the experimental results.

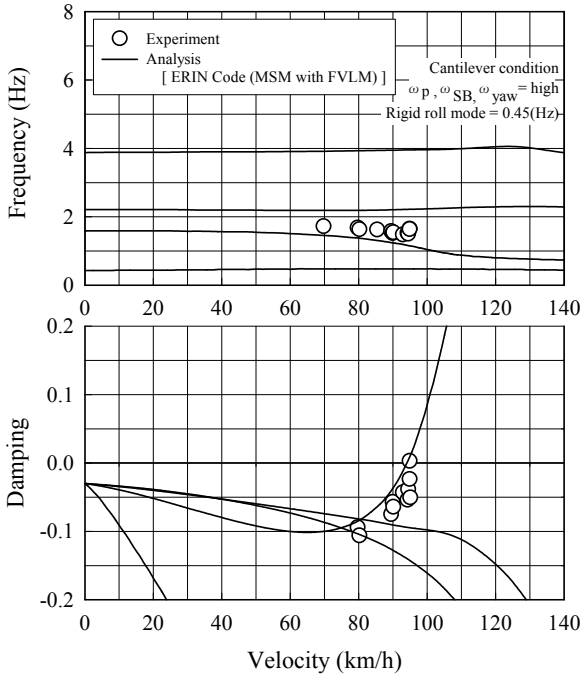

Fig.28 Free-free antisymmetric flutter test results

Concluding Remarks

Analytical and experimental studies were conducted to investigate the flutter characteristics of an over-the-wing engine-mount configuration. The following results were obtained:

1. The flutter characteristics of the over-the-wing engine mount configuration are influenced by the engine-pylon vibration characteristics. The flutter speed becomes highest when the engine-pylon side-bending frequency is close to the uncouple 1st wing torsion frequency (about 0.9 to 1.0 times the uncouple 1st wing torsion frequency). The flutter speed also becomes highest when the engine-pylon yawing frequency is about 0.9 times the uncouple 1st wing torsion frequency. When the engine-pylon pitching frequency is about 1.25 times the uncouple 1st wing bending frequency, the flutter speed is lowest and the flutter speed increases above and below this frequency ratio.

2. For the over-the-wing engine-mount configuration, the effects of the aerodynamic loads and interference due to the engine-nacelle installation over the wing are small at transonic speeds. The Mach number at which the lower limit of the transonic flutter boundary occurs for the over-the-wing engine mount configuration is about 0.03 higher than that for the clean-wing configuration. Overall the transonic dip characteristics of the over-the-wing engine mount configuration are similar to those of the clean-wing configuration.

3. The symmetric flutter mode is more critical than the antisymmetric flutter mode for the over-the-wing engine mount configuration. The symmetric flutter mode must be carefully evaluated during the design of an over-the-wing engine-mount configuration.

4. The predicted flutter speed from the ERIN Code using a modified strip analysis with a steady-state Euler solution is in good agreement with the measured transonic flutter results.

References

1. Fujino, M ; Wave-Drag Characteristics of an Over-the-Wing Nacelle Business-Jet Configuration, AIAA 2003-0933, January 2003

2. Nakai, E. et al.; Some Effects of Systematically-Varied Location of a Concentrated Mass on Transonic Flutter Characteristics of Sweptback Thin Cantilever Wings, NAL TR-226, November 1970

3. Hiraki, T. et al. ; Vibration and Flutter of the Wing of a Twin-Engine Aircraft, Journal of the Japan Society for Aeronautical and Space Sciences, Vol.19, No.211, August 1971

4. Forsching, H and Knaack, J. M. ; Parametric Study of the Flutter Stability of a Semi-Rigid 3-D Wing-With-Engine Nacelle Model in Subsonic Flow, Journal of Fluids and Structures, 7, pp567-pp596, 1993

5. Scanlan, R.H. and Rosenbaum, R.; Introduction to the study of aircraft vibration and flutter, 1968

6. Yates, E.C. Jr. ; Calculation of Flutter Characteristics for Finite-Span Swept or Unswept Wings at Subsonic and Supersonic Speeds by Modified Strip Analysis, NACA RM L57L10, 1958

7. Albano, E. and Rodden, W. P.; A Doublet-Lattice Method for Caluculating Lift Distributions on Oscillating Surfaces in Subsonic Flows, AIAA Journal, Vol.7, No.2, February 1969

8. Strash, D. J. and Tidd, D. M.,"MGAERO User's Manual", Analytical Methods Inc., Redmond, WA

9. Tidd. D. M., et al., "Application of an Efficient 3-D Multi-Grid Euler Method to Complete Aircraft Configurations", AIAA-91-3236, AIAA 9th Applied Aerodynamics Conference, 1991

10. Epstein "Multigrid Euler Solver About Arbitrary Aircraft Configurations with Cartesian Grids and Local Refinement", AIAA-89-1960-CP, 1989

11. Fujino, M, et al.; Natural-Laminar-Airfoil Development for the Honda Jet, AIAA 2002-2932, June 2002

Acknowledgement

The author wishes to thank Honda R&D for permission to publish this paper and my colleagues for their valuable assistance. The author also wishes to gratefully acknowledge the assistance of Dr.Nakamichi and Mr.Kikuchi of the National Aeronautical Lab.